Supporting Information

Platinum Single-atom Anchored on Covalent Organic Framework: Boosting Active Sites for Photocatalytic Hydrogen Evolution

Pengyu Dong[†,#], Yan Wang[‡,#], Aicaijun Zhang[‡], Ting Cheng[†], Xinguo Xi[*,‡], and Jinlong Zhang*[*,§]*

[†]Key Laboratory for Advanced Technology in Environmental Protection of Jiangsu Province, Yancheng Institute of Technology, Yancheng 224051, P. R. China

[‡]School of Chemistry and Chemical Engineering, Yancheng Institute of Technology, Yancheng 224051, P. R. China

[§]Key Laboratory for Advanced Materials and Institute of Fine Chemicals, School of Chemistry & Molecular Engineering, East China University of Science and Technology, 130 Meilong Road, Shanghai 200237, P. R. China

Contents

1. Catalyst Characterizations: The morphology was investigated by SEM (FEI Nova NanoSEM 450), TEM (JEOL JEM-2100F, 200 kV) equipped with EDS (X-MaxN 80T IE250), and HAADF-STEM (FEI Titan Themis 60-300), which was performed with a spherical aberration corrector operating at an accelerating voltage of 200 kV. The crystal structures of the obtained samples were identified by PXRD (PANalytical X'Pert^3 Powder). FTIR spectra were recorded on a NICOLET NEXUS-670, and the samples were dried at 60 °C for 8 h before testing. Raman spectra were obtained on Thermo Fischer DXR by using a 532 nm laser as the light source. XPS and UPS analysis (Thermo Scientific, ESCALAB 250Xi) was measured by an X-ray source with a hemispherical electron energy analyzer and an Al Kα (hν = 1486.6 eV). N_2 adsorption-desorption isotherms were carried out by Micromeritics ASAP 2020 analyzer at 77 K. XAFS spectra were performed on the beamline BL07A1 in NSRRC (Taiwan), in which the radiation was monochromatized by a Si (111) double-crystal monochromator, and the data reduction and analysis of XANES and FT-EXAFS spectra were completed by using Athena software through the technical support provided by Ceshigo Research Service: "www.ceshigo.com". ICP−OES was conducted on an OPTIMA 5300 DV spectrometer. UV−Vis DRS (Shimadzu, UV-3600) were recorded using $BaSO_4$ as a reference. PL spectra and PL decay profiles (FLS980, Edinburgh, UK) were performed at room temperature using 365 nm as the excitation source. EIS, Mott−Schottky plots, and I−t profiles were conducted on the CHI660E electrochemical workstation with a standard three-electrode system, where the indium tin oxide (ITO) coated with photocatalyst as the working electrode, Ag/AgCl (saturated KCl) electrode as the reference electrode, and Pt plate as the counter electrode. The 0.5 M Na_2SO_4 solution was employed as the electrolyte. Typical preparation of film of photocatalyst-coated ITO electrode was carried out according to the literature.[1]

2. Supplementary Figures and Tables

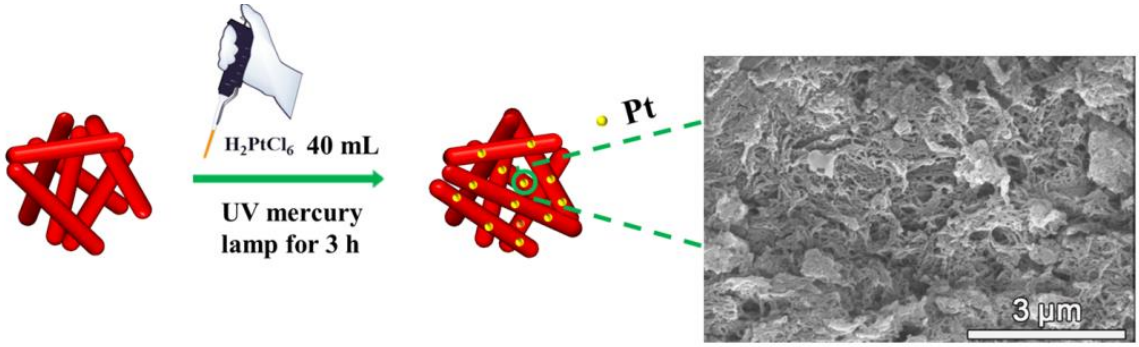

Scheme S1. Schematic illustration of the preparation process of 3% Pt NPs/TpPa-1.

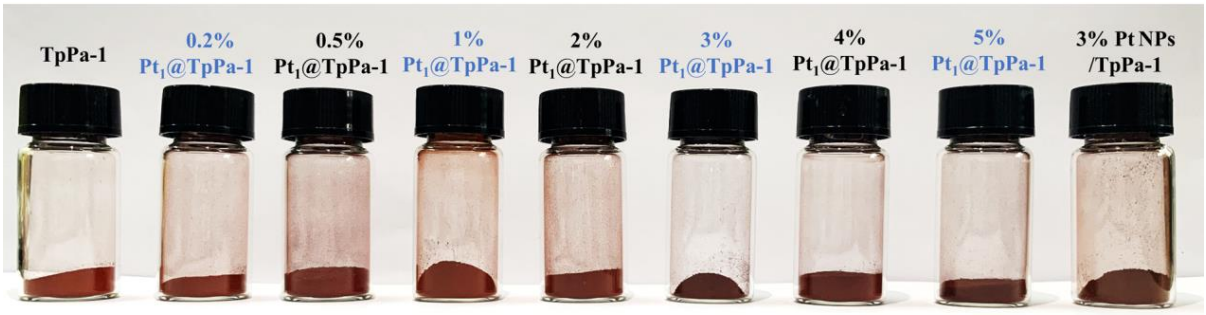

Figure S1. The photographs of the obtained samples of TpPa-1, 3% Pt NPs/TpPa-1, and Pt_1@TpPa-1 with various loading amounts of single-atom Pt.

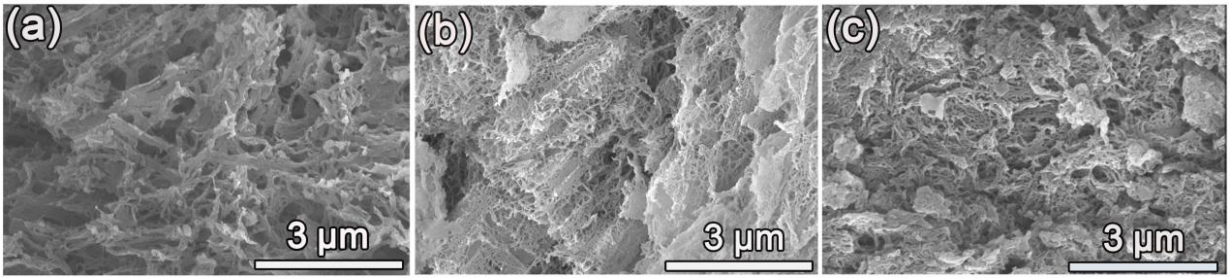

Figure S2. SEM images of (a) TpPa-1, (b) 3% Pt_1@TpPa-1, and (c) 3% Pt NPs/TpPa-1.

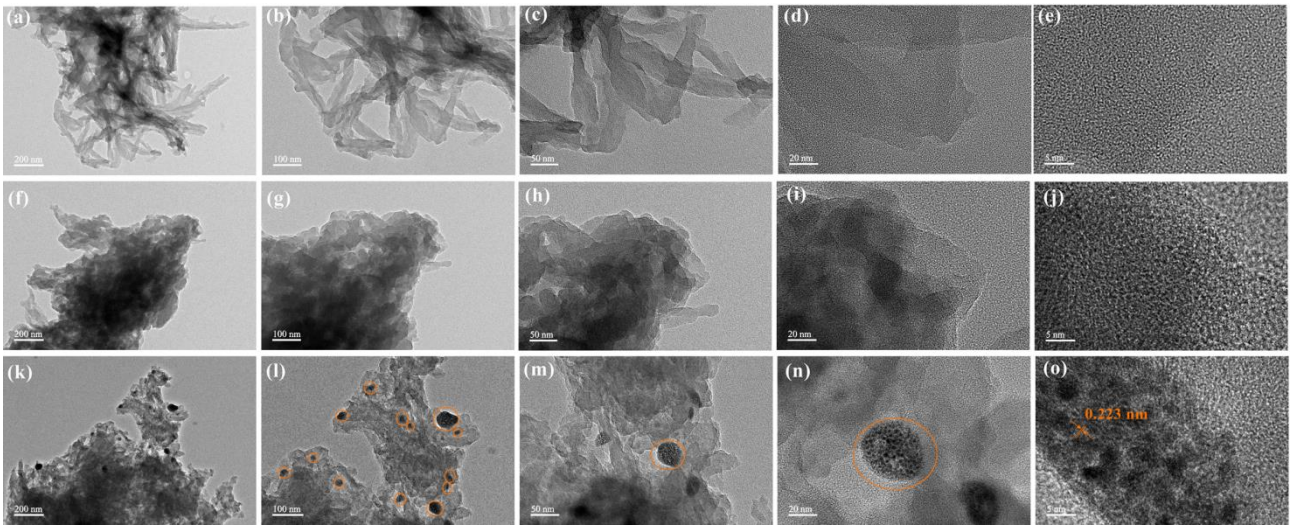

Figure S3. TEM and HRTEM images of pure TpPa-1 (a−e), 3% Pt_1@TpPa-1 (f−j), and 3% Pt NPs/TpPa-1 (k−o).

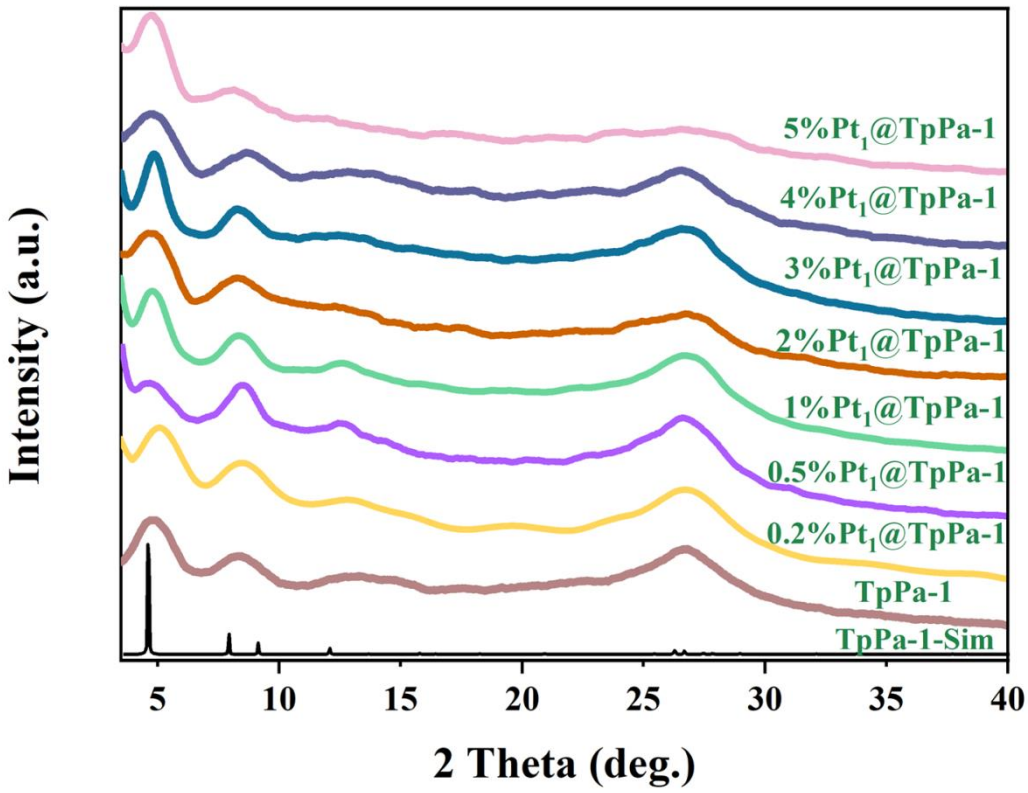

Figure S4. PXRD patterns of all of the prepared Pt_1@TpPa-1 (with different contents of single-atom Pt) samples and the simulated XRD pattern of TpPa-1.

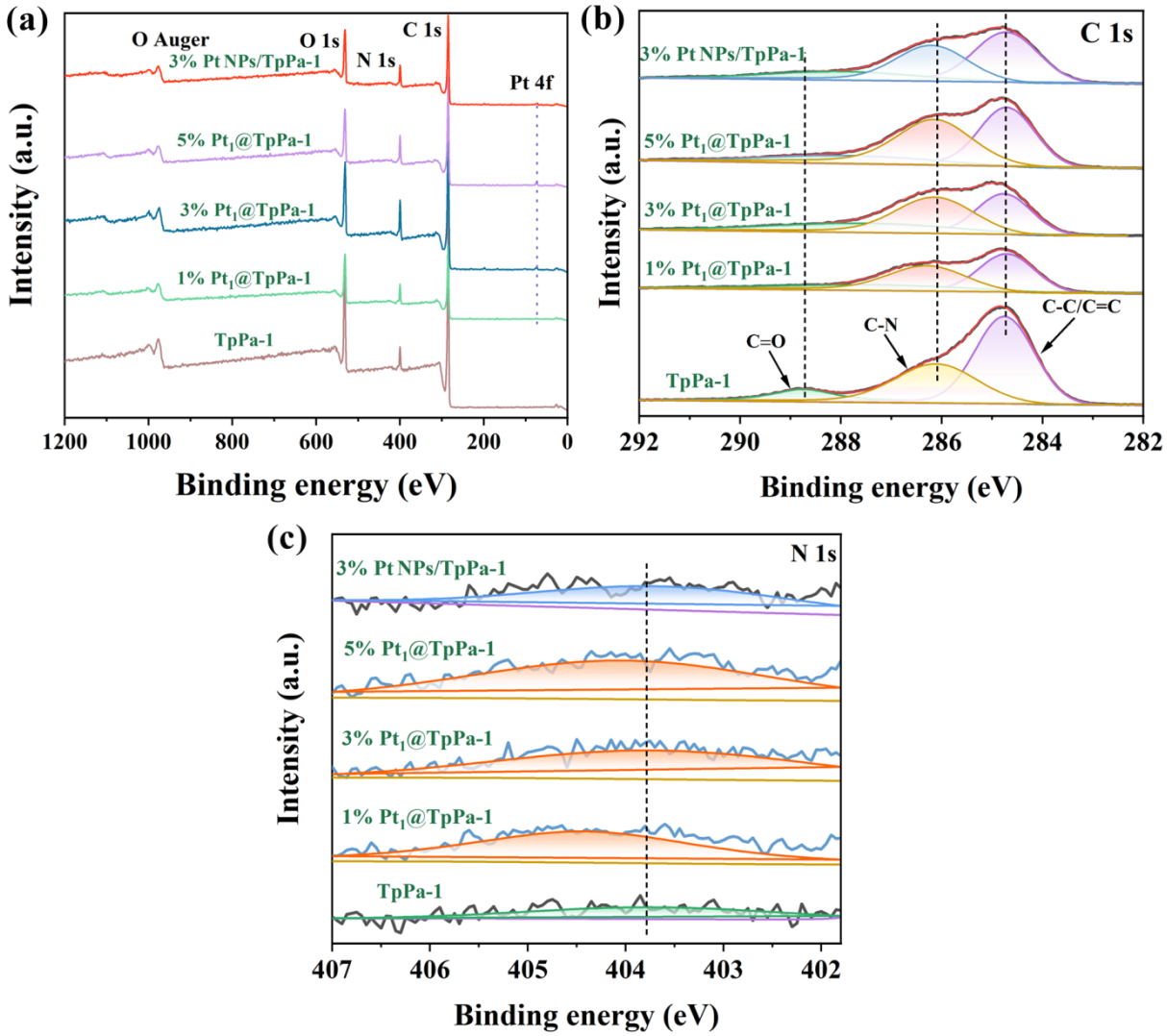

Figure S5. (a) XPS survey spectra, (b) C 1s high-resolution XPS spectra, (c) the enlarged part of high-resolution N 1s XPS spectra of as-prepared samples at 407−401.5 eV.

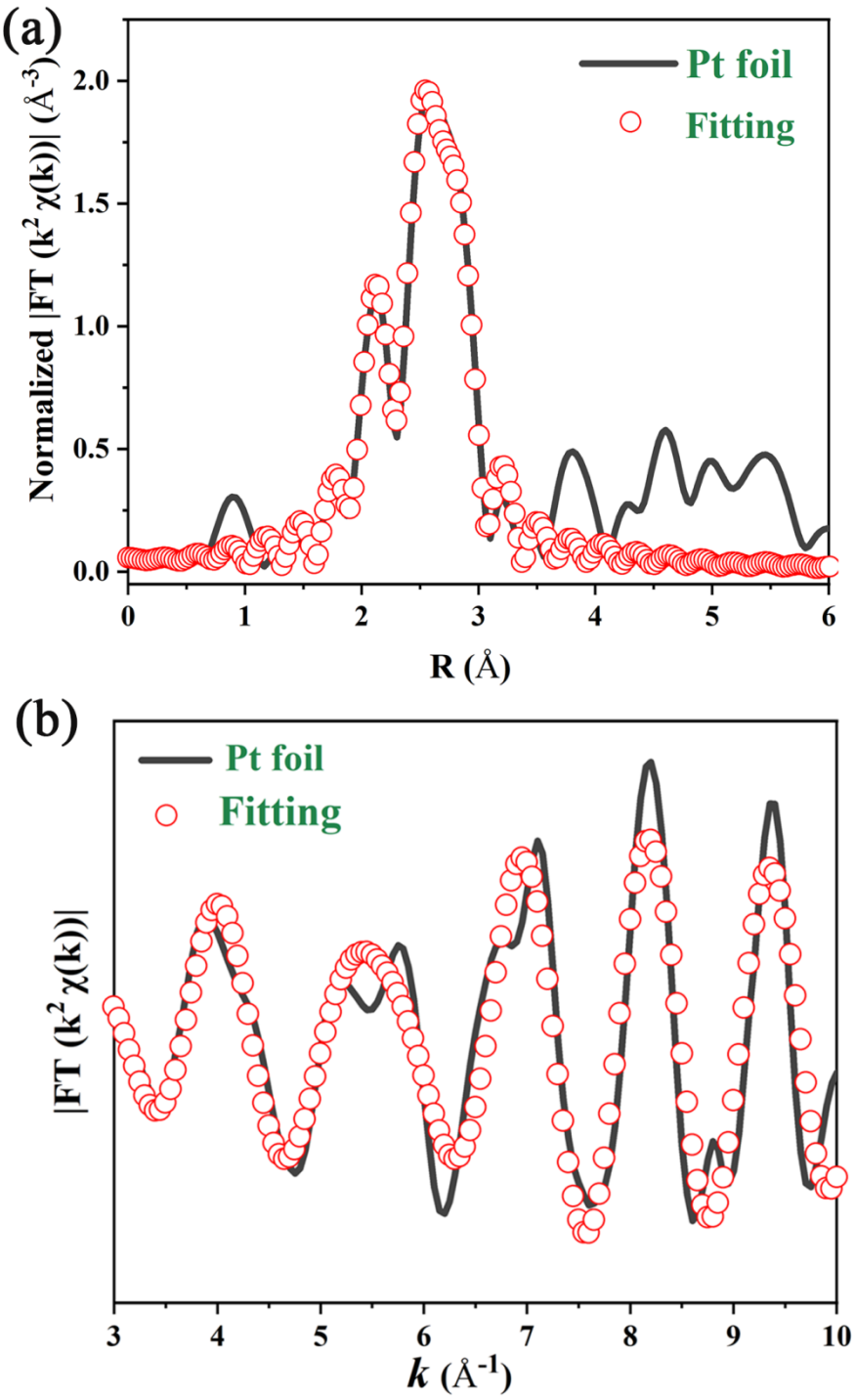

Figure S6. Fourier-transformed magnitudes of Pt L-edge EXAFS spectra in *R* space (a) and *k* space (b) for Pt foil.

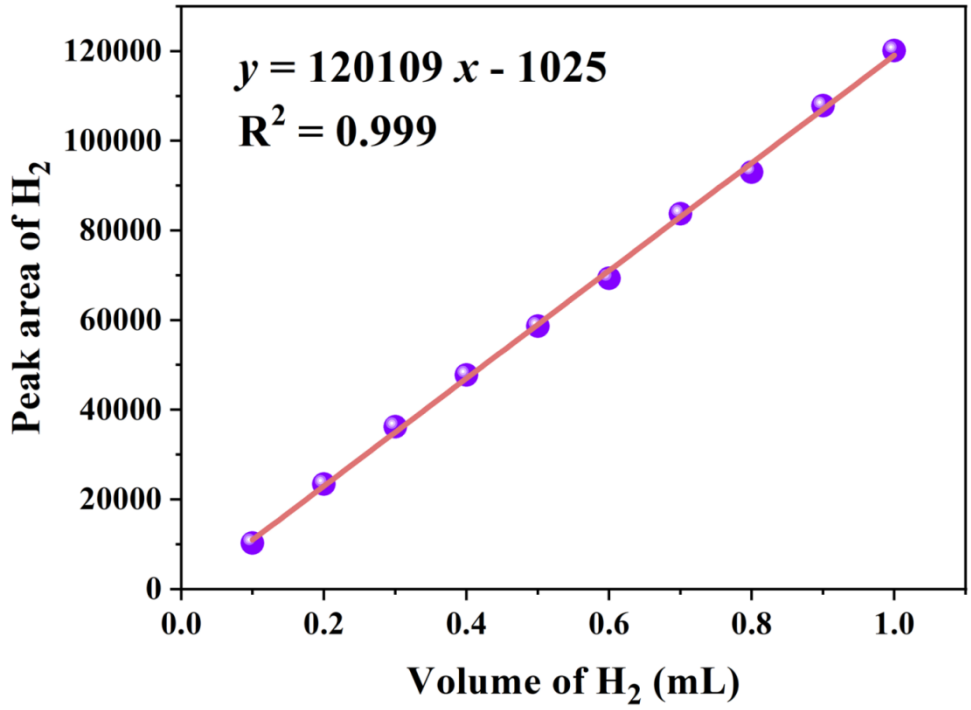

Figure S7. The standard curve of H_2 production.

The standard calibration curve of H_2 detection is shown in Figure S7. The generated amount of H_2 evolved was analyzed by chromatography with a known concentration of H_2 as standard gas. According to the fitted standard curve, the relationship between the peak area and the volume of H_2 evolved can be expressed as Equation S1:

$$y = 120109x - 1025$$

Where y is the peak area corresponded to H_2 in the chromatography, and x is the volume of H_2 evolved (mL).

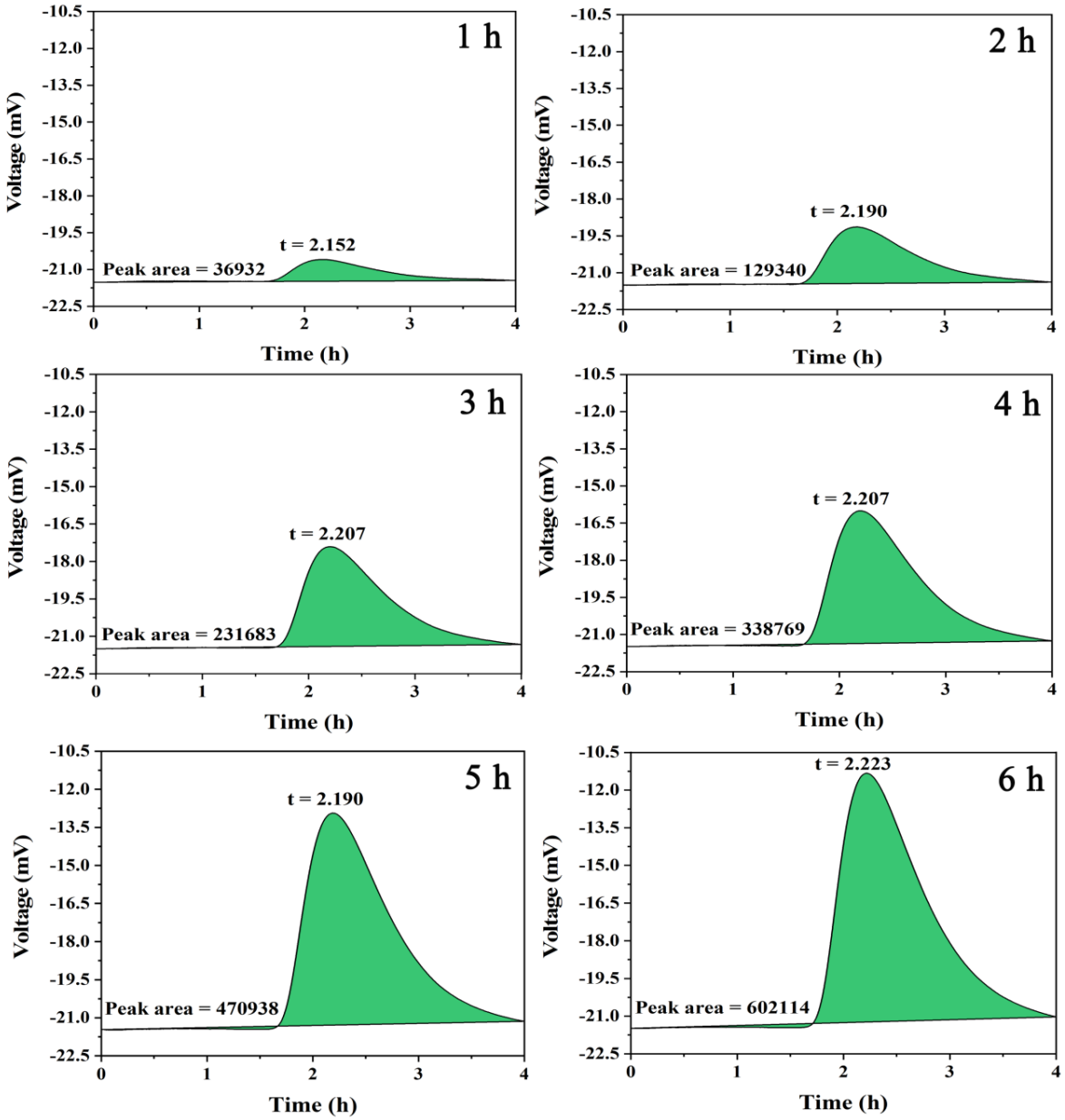

Figure S8. The chromatogram of H_2 evolved over 3% Pt_1@TpPa-1.

An example of the H_2 evolved chromatogram is given in Figure S8, which illustrates the process of the peak area over 3% Pt_1@TpPa-1 photocatalyst under visible light irradiation. The amount of H_2 evolved was determined at an interval of 1 h using an online gas chromatograph instrument with a thermal conductivity detector. The measured peak area was converted into the H_2 evolution rate according to the standard curve (Equation S1).

The number of generated moles (mmol) of H_2 generated can be expressed as Equation S2.

$$n = \frac{V}{22.4}$$

Where n is the number of moles (mmol) of H_2 produced, V is the hydrogen volume evolved (mL), and 22.4 is the molar volume of the gas (mL $mmol^{-1}$).

Moreover, the number of moles of hydrogen produced per mass of photocatalyst (mmol g^{-1}) can be expressed as Equation S3:

$$C(H_2) = \frac{n}{m}$$

Where $C(H_2)$ is the number of moles of hydrogen produced per mass of photocatalyst (mmol g^{-1}), and m is the amount of photocatalyst (g) added in the photocatalytic reactor.

Furthermore, the mean value of the amount of H_2 produced per unit mass of photocatalyst and per unit time (mmol g^{-1} h^{-1}) can be evaluated according to Equation S4−S5.

$$P(H_2) = \frac{C(H_2)}{t}$$

$$\bar{P}(H_2) = \frac{\sum_{i=1}^{n=6} P_i(H_2)}{n}$$

Where P is the amount of H_2 produced per gram of photocatalyst per hour (mmol g^{-1} h^{-1}), and $\overline{P}$ is the mean value of P (mmol g^{-1} h^{-1}).

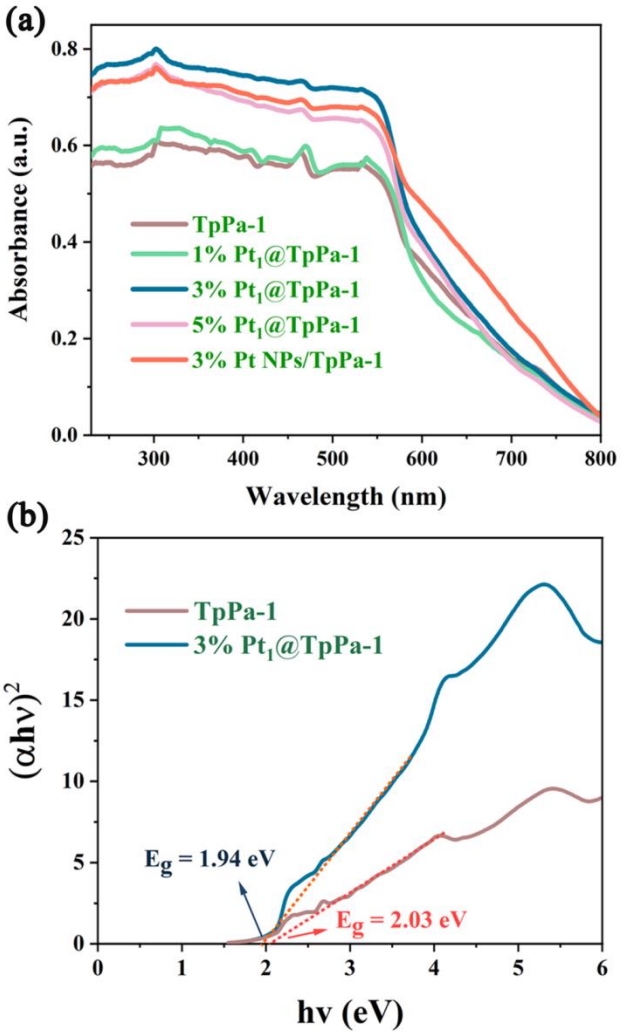

Figure S9. (a) UV−Vis DRS spectra of TpPa-1, 3% Pt NPs/TpPa-1, and Pt_1@TpPa-1 (1%, 3%, and 5%). (b) Tauc plots of TpPa-1 and 3% Pt_1@TpPa-1.

The band gap energy (E_g) was calculated using the Tauc's Equation:

$$\alpha h\nu = A(h\nu - Eg)^n \qquad \text{(S6)}$$

where α represents absorption coefficient, A represents the absorption constant, and n represents a constant which depends on the probability of transition; it takes the values 1/2 and 2 for direct allowed and indirect allowed transitions, respectively. Because TpPa-1 is a direct band gap semiconductor,[2] E_g of the samples was estimated from the intercept of the tangent in the plots of $(\alpha h\nu)^2$ versus photon energy $(h\nu)$.

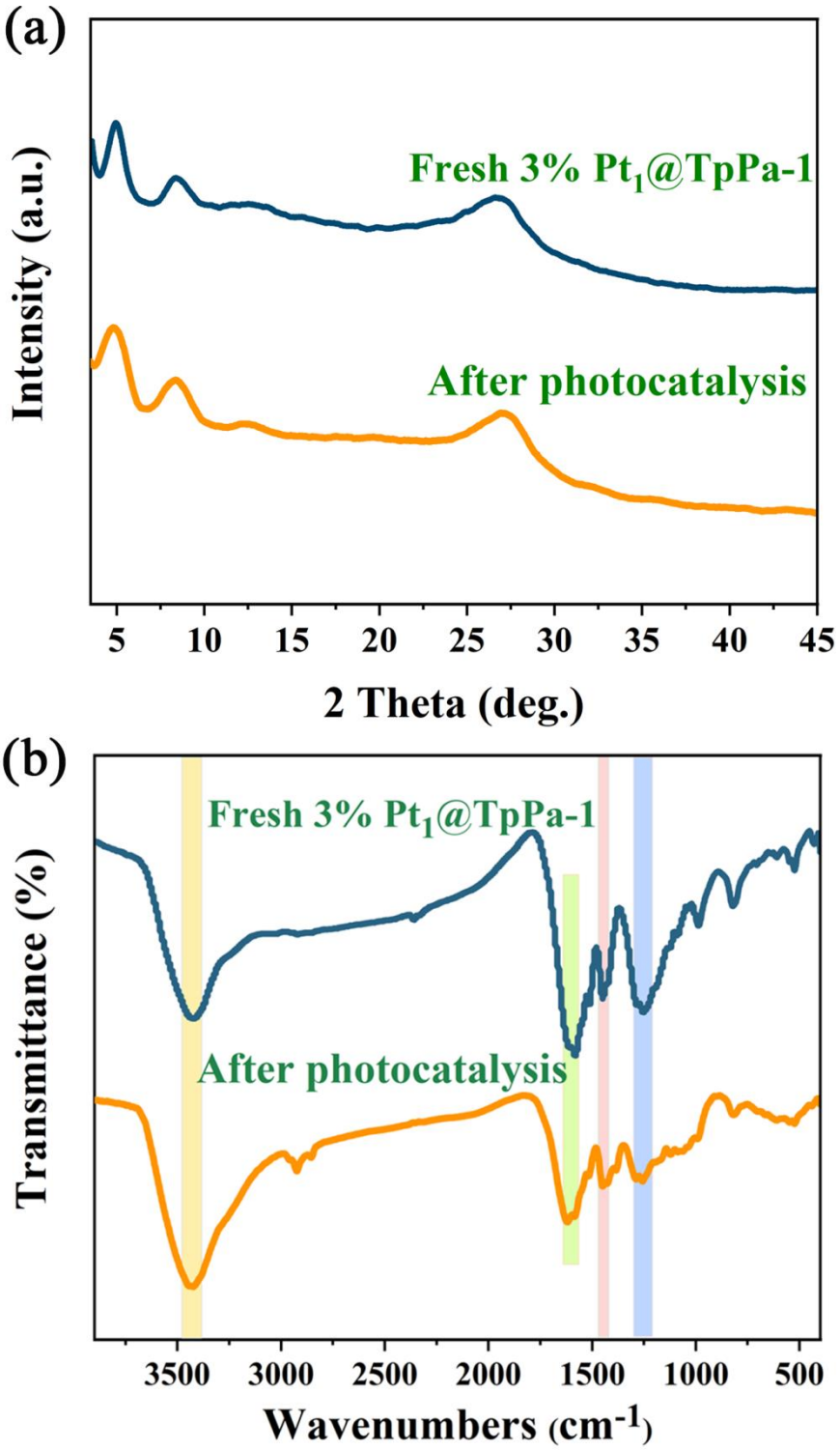

Figure S10. (a) XRD patterns, and (b) FTIR spectra of 3% Pt_1@TpPa-1 before and after photocatalysis.

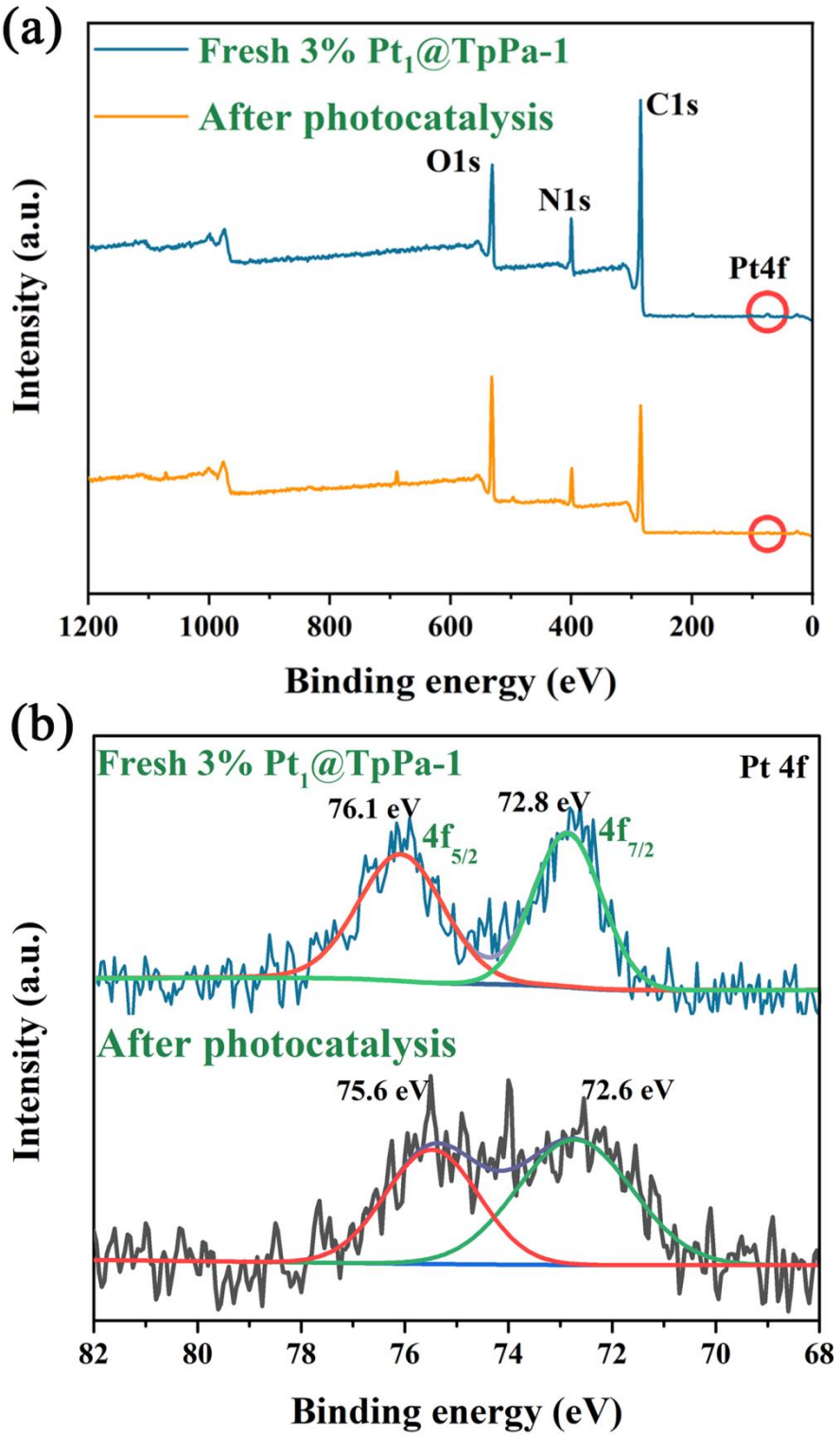

Figure S11. (a) The XPS survey spectra, (b) high-resolution Pt 4f XPS spectra of 3% Pt_1@TpPa-1 before and after photocatalysis.

Calculation of the electron transfer rate (k_{ET}) from PL decay lifetimes:

The electron transfer rate (k_{ET}) of the TpPa-1 and 3% Pt_1@TpPa-1 was calculated according to Equation S7.

$$k_{ET} = \frac{1}{\tau_{3\%\ Pt_1@TpPa\text{-}1}} - \frac{1}{\tau_{TpPa\text{-}1}}$$

Where the $\tau_{3\%\ Pt1@TpPa\text{-}1}$ and $\tau_{TpPa\text{-}1}$ represent the time-resolved fluorescence decay lifetimes, respectively, which are 0.27 and 0.50 ns. Thus, the k_{ET} can be calculated to be 1.71×10^{9} s^{-1}.

Calculation of the energy levels from UPS spectra:

The energy level of valence band maximum (E_{VBM}) can be calculated using Equation S8:[3-6]

$$E_{(VBM)} = h\nu - (E_{cutoff} - E_{onset})$$

Where $h\nu$ is the incident photon energy (21.22 eV), E_{cutoff} is the high binding energy cutoff, and E_{onset} is the onset energy in the valence-band region.

The energy level of conduction band minimum (E_{CBM}) can be calculated using Equation S9:

$$E_{(CBM)} = E_{(VBM)} - E_g$$

Where and E_g is the band gap of the sample.

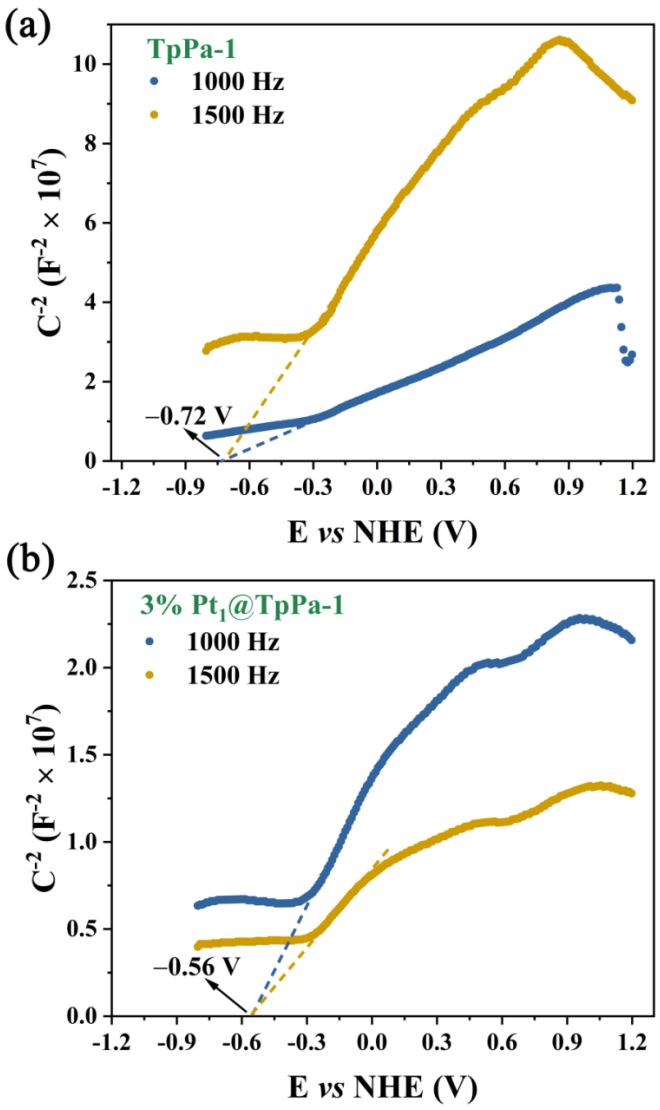

Figure S12. Mott−Schottky plots of (a) TpPa-1 and (b) 3% Pt_1@TpPa-1 measured with Ag/AgCl as the reference electrode in dark at 1000 and 1500 Hz.

The measured potentials *vs.* Ag/AgCl can be converted to normal hydrogen electrode (NHE) scale using Equation S10: [7, 8]

$$E_{(\mathrm{NHE})} = E_{(\mathrm{Ag/AgCl})} + 0.197$$

The energy positions of band edges in the electrochemical scale (V) can be converted from the values in absolute vacuum scale (eV) using Equation S11:[9]

$$E\ (\mathrm{eV}) = -4.5 - E_{(\mathrm{NHE})}\ (\mathrm{V})$$

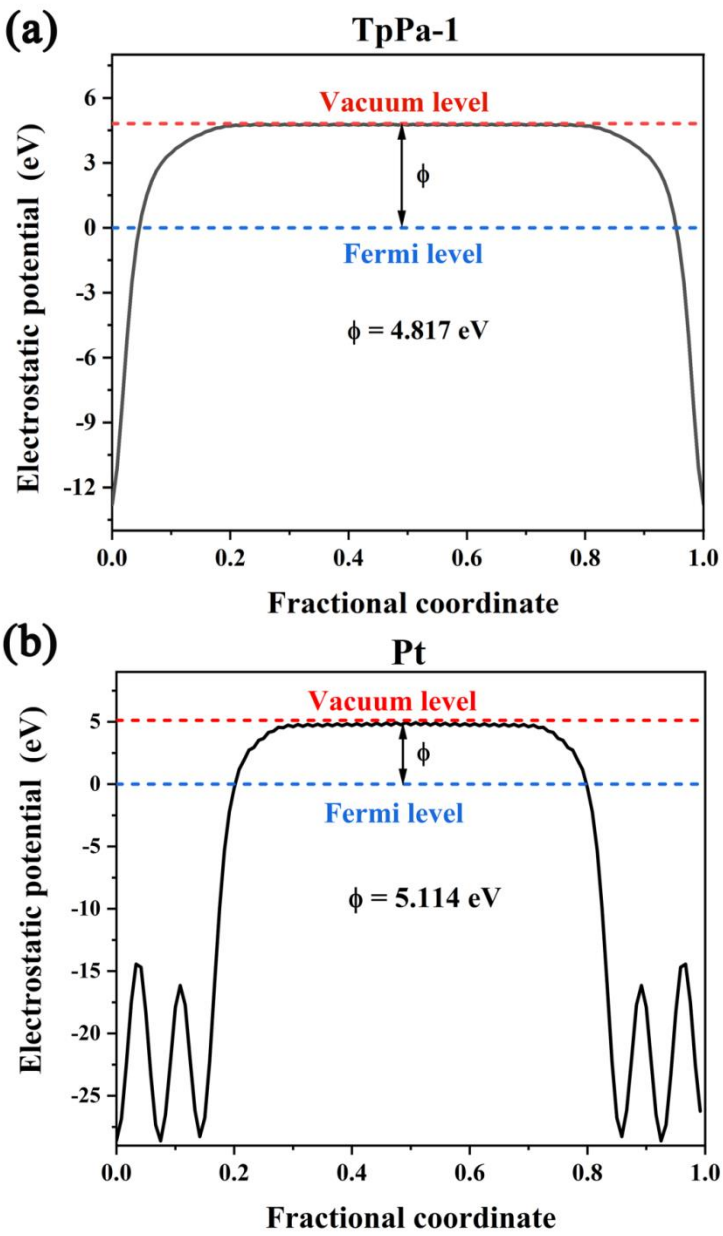

Figure S13. The calculated work function of the surface of (a) TpPa-1 and (b) {−100} surface of Pt.

Table S1. BET surface areas, pore volumes, and average pore sizes of the as-prepared samples.

Sample	BET surface area ($m^2\ g^{-1}$)	Pore volume ($cm^3\ g^{-1}$)	Average pore size (nm)
TpPa-1-COF	327	0.38	9.35
1% Pt_1@TpPa-1	301	0.33	7.44
3% Pt_1@TpPa-1	326	0.39	8.42
5% Pt_1@TpPa-1	374	0.43	9.57
3% Pt NPs/TpPa-1	306	0.34	7.59

Table S2. Structural parameters obtained from the Pt L_3-edge EXAFS fitting.

Sample	Shell	[a]*N*	[b]*R*(Å)	[c]σ^2 (Å^2)	[d]ΔE_0 (eV)	*R*, %
Pt foil	Pt−Pt	12	2.76±0.01	0.0049	7.5±0.7	0.0076
Pt NPs/TpPa-1	Pt−O/N	4.3±0.8	2.02±0.01	0.002	9.55±0.91	0.011
	Pt−Pt	6	3.11±0.03	0.003	9.55±0.91	0.011
	Pt−C	3	3.31±0.03	0.0129		
Pt_1@TpPa-1	Pt−N	1	2.06±0.01	0.0002	9.0±1.2	0.0073
	Pt−Cl	2	2.30±0.01	0.00052		

[a]*N*: coordination numbers, [b]*R*: bond distance, [c]σ^2: Debye−Waller factors, [d]ΔE_0: the inner potential correction. *R* factor (%): degree of the fitting. S_0^2 was set to be 0.82 according to the experimental EXAFS fitting of the reference Pt foil by fixing *N* as the known crystallographic value. Error bounds (accuracies) were estimated as *N*, ±5%, *R*, ±1%.

The obtained XAFS data was performed using Athena (version 0.9.26) software for background, pre-edge line, and post-edge line calibrations. Then Fourier transformed fitting was carried out. The k^2 weighting, the *k*-range of 3−12.116 Å^{-1} (3−14.263 Å^{-1} for Pt sample; 3−12 Å^{-1} for PtO_2 sample), and *R* range of 1−3 Å were utilized for all of the fittings. The four parameters, coordination number, bond length, Debye−Waller factor, and E_0 shift (*N*, *R*, σ^2, and ΔE_0) were fitted without anyone was fixed, constrained, or correlated.

For Wavelet Transform analysis, the χ(*k*) exported from Athena was imported into the Hama Fortran code. The parameters were listed as follow: *k* range, 0−11.95 Å^{-1} (0−12 Å^{-1} for Pt sample); *k* weight, 2; *R* range, 1−4 Å; and Morlet function with κ=10, σ=1 was employed as the mother.

Table S3. Summary of H_2 evolution performance of some typical COF-based and single atom-based photocatalytic systems.

Photocatalyst	Co-catalyst	Sacrificial electron donor	Solvent	Illumination	Activity (μmol g^{-1} h^{-1})	Overall H_2 production (μmol m^{-2})	AQE (%) (mass of photocatalyst)	TON (time)	TOF (h^{-1})	Reference
TpPa-1	0.72 wt% Pt_1 (ICP)	SA	PBS	≥420 nm	719	17.24 (6 h)	0.38 (420 nm, 10 mg)	304 (6 h)	19.5	This work
TP-BDDA	3 wt% Pt	TEOA	H_2O	≥395 nm	324	4.3[a] (10 h)	1.3 (420 nm, 10 mg); 1.8 (520 nm)	42.3[a] (10 h)	2.1[a]	[10]
A-TEBPY	2.2 wt% Pt	TEOA	H_2O	AM 1.5	98	3.1[a] (22 h)	–	37.23[a] (22 h)	0.87[a]	[11]
ZnPor-DETH-COF	8 wt% Pt	TEOA	PBS	>400 nm	413	4.1[a] (10 h)	0.063 (450 nm, 0.5 mg)	20.23[a] (10 h)	1.01[a]	[12]
g-$C_{18}N_3$-COF	3 wt% Pt	Ascorbic acid	H_2O	≥420 nm	292	1.01[a] (4 h)	1.06 (420 nm, 50 mg)	15.34[a] (4 h)	1.90[a]	[13]
N2-COF	Co-1[b]	TEOA	ACN/H_2O	AM 1.5	782	–	0.16 (400 nm, 5 mg)	54.4 (20 h)	3.96	[14]
TpDTz	NiME cluster	TEOA	H_2O	AM 1.5	941	–	0.2 (400 nm, 5 mg)	>103 (70 h)	2.3	[15]
TFPT-COF	2.2 wt% Pt	TEOA	H_2O	>420 nm	1970	–	2.2 (400 nm, 10 mg)	–	15.7[a]	[16]
N3-COF	0.68 wt% Pt (ICP)	TEOA	PBS	≥420 nm	1703	9.11[a] (8 h)	0.44 (450 nm, 10 mg)	781[a] (8 h)	48.8[a]	[17]
COF-alkene	3 wt% Pt	TEOA	H_2O	>420 nm	2330	65.40[a] (5 h)	6.7 (420 nm, 20mg)	157.3[a] (5 h)	15.14	[18]
COF-imide	3 wt% Pt	TEOA	H_2O	>420 nm	34	0.03[a] (5 h)	–	0.65[a] (5 h)	0.22[a]	[18]

Table S3 (continued)

Photocatalyst	Co-catalyst	Sacrificial electron donor	Solvent	Illumination	Activity (μmol g^{-1} h^{-1})	Overall H_2 production (μmol m^{-2})	AQE (%) (mass of photocatalyst)	TON (time)	TOF (h^{-1})	Reference
COF-imine	3 wt% Pt	TEOA	H_2O	>420 nm	12	0.17[a] (5 h)	–	0.54[a] (5 h)	0.08[a]	[18]
CTF-HUST-2	3 wt% Pt	TEOA	H_2O	>420 nm	2647	10.56[a] (3h)	–	104.0[a] (3h)	17.2[a]	[19]
Al-TCPP-0.1Pt	0.07 wt% Pt_1 (ICP)	TEOA	ACN/H_2O	>380 nm	129	–	–	261.8[a] (5 h)	35	[20]
HNTM-Ir/Pt	1.05 wt% Ir_1 and 2.54 wt% Pt_1 (ICP)	TEOA	ACN/H_2O	>400 nm	201.9	1.18[a] (5 h)	–	10.9[a] (5 h）	1.10[a]	[21]
Co_1-phosphide/PCN	0.4 wt% Co_1 (ICP)	–	H_2O	>300 nm	410.3	–	3.6 (420 nm, 20 mg)	–	6.04[a]	[22]

[a]The values were calculated based on the data in the corresponding References.

[b]Co-1: $[Co(dmgH)_2pyCl]$

References

1. Wu, T.; Zhang, Q.; Hou, Y.; Wang, L.; Mao, C.; Zheng, S. T.; Bu, X.; Feng, P., Monocopper Doping in Cd-In-S Supertetrahedral Nanocluster via Two-Step Strategy and Enhanced Photoelectric Response. *J. Am. Chem. Soc.* **2013,** *135* (28), 10250-10253.

2. Zhang, F. M.; Sheng, J. L.; Yang, Z. D.; Sun, X. J.; Tang, H. L.; Lu, M.; Dong, H.; Shen, F. C.; Liu, J.; Lan, Y. Q., Rational Design of MOF/COF Hybrid Materials for Photocatalytic H_2 Evolution in the Presence of Sacrificial Electron Donors. *Angew. Chem. Int. Ed.* **2018,** *57* (37), 12106-12110.

3. Liu, J.; Liu, Y.; Liu, N.; Han, Y.; Zhang, X.; Huang, H.; Lifshitz, Y.; Lee, S. T.; Zhong, J.; Kang, Z., Metal-Free Efficient Photocatalyst for Stable Visible Water Splitting via a Two-Electron Pathway. *Science* **2015,** *347* (6225), 970-974.

4. Pan, J.; Wei, C.; Wang, L.; Zhuang, J.; Huang, Q.; Su, W.; Cui, Z.; Nathan, A.; Lei, W.; Chen, J., Boosting the Efficiency of Inverted Quantum Dot Light-Emitting Diodes by Balancing Charge Densities and Suppressing Exciton Quenching through Band Alignment. *Nanoscale* **2018,** *10* (2), 592-602.

5. Wang, S.; Xu, M.; Peng, T.; Zhang, C.; Li, T.; Hussain, I.; Wang, J.; Tan, B., Porous Hypercrosslinked Polymer-TiO_2-Graphene Composite Photocatalysts for Visible-Light-Driven CO_2 Conversion. *Nat. Commun.* **2019,** *10* (1), 676.

6. Hou, Y.; Du, X.; Scheiner, S.; McMeekin, D. P.; Wang, Z.; Li, N.; Killian, M. S.; Chen, H.; Richter, M.; Levchuk, I.; Schrenker, N.; Spiecker, E.; Stubhan, T.; Luechinger, N. A.; Hirsch, A.; Schmuki, P.; Steinrück, H.-P.; Fink, R. H.; Halik, M.; Snaith, H. J.; Brabec, C. J., A Generic Interface to Reduce the Efficiency-Stability-Cost Gap of Perovskite Solar Cells. *Science* **2017,** *358* (6367), 1192-1197.

7. Xiao, J. D.; Han, L.; Luo, J.; Yu, S. H.; Jiang, H. L., Integration of Plasmonic Effects and Schottky Junctions into Metal-Organic Framework Composites: Steering Charge Flow for Enhanced Visible-Light Photocatalysis. *Angew. Chem. Int. Ed. Engl.* **2018,** *57* (4), 1103-1107.

8. Kanan, M. W.; Nocera, D. G., In Situ Formation of an Oxygen-Evolving Catalyst in Neutral Water Containing Phosphate and Co^{2+}. *Science* **2008,** *321* (5892), 1072-1075.

9. Xu, Y.; Schoonen, M. A. A., The Absolute Energy Positions of Conduction and Valence Bands of Selected Semiconducting Minerals. *Am. Mineral.* **2000,** *85* (3-4), 543-556.

10. Pachfule, P.; Acharjya, A.; Roeser, J.; Langenhahn, T.; Schwarze, M.; Schomäcker, R.; Thomas, A.; Schmidt, J., Diacetylene Functionalized Covalent Organic Framework (COF) for Photocatalytic Hydrogen Generation. *J. Am. Chem. Soc.* **2018,** *140* (4), 1423-1427.

11. Stegbauer, L.; Zech, S.; Savasci, G.; Banerjee, T.; Podjaski, F.; Schwinghammer, K.; Ochsenfeld, C.; Lotsch, B. V., Tailor−Made Photoconductive Pyrene−Based Covalent Organic Frameworks for Visible−Light Driven Hydrogen Generation. *Adv. Energy Mater.* **2018,** *8* (24), 1703278.

12. Chen, R.; Wang, Y.; Ma, Y.; Mal, A.; Gao, X.-Y.; Gao, L.; Qiao, L.; Li, X.-B.; Wu, L.-Z.; Wang, C., Rational Design of Isostructural 2D Porphyrin-Based Covalent Organic Frameworks for Tunable Photocatalytic Hydrogen Evolution. *Nat. Commun.* **2021,** *12* (1), 1354.

13. Wei, S.; Zhang, F.; Zhang, W.; Qiang, P.; Yu, K.; Fu, X.; Wu, D.; Bi, S.; Zhang, F., Semiconducting 2D Triazine-Cored Covalent Organic Frameworks with Unsubstituted Olefin Linkages. *J. Am. Chem. Soc.* **2019,** *141* (36), 14272-14279.

14. Banerjee, T.; Haase, F.; Savasci, G.; Gottschling, K.; Ochsenfeld, C.; Lotsch, B. V., Single-Site Photocatalytic H_2 Evolution from Covalent Organic Frameworks with Molecular Cobaloxime Co-Catalysts. *J. Am. Chem. Soc.* **2017,** *139* (45), 16228-16234.

15. Biswal, B. P.; Vignolo-González, H. A.; Banerjee, T.; Grunenberg, L.; Savasci, G.; Gottschling, K.; Nuss, J.; Ochsenfeld, C.; Lotsch, B. V., Sustained Solar H_2 Evolution from a Thiazolo[5,4-D]Thiazole-Bridged Covalent Organic Framework and Nickel-Thiolate Cluster in Water. *J. Am. Chem. Soc.* **2019,** *141* (28), 11082-11092.

16. Stegbauer, L.; Schwinghammer, K.; Lotsch, B. V., A Hydrazone-Based Covalent

Organic Framework for Photocatalytic Hydrogen Production. *Chem. Sci.* **2014,** *5* (7), 2789-2793.

17. Vyas, V. S.; Haase, F.; Stegbauer, L.; Savasci, G.; Podjaski, F.; Ochsenfeld, C.; Lotsch, B. V., A Tunable Azine Covalent Organic Framework Platform for Visible Light-Induced Hydrogen Generation. *Nat. Commun.* **2015,** *6*, 8508.

18. Mo, C.; Yang, M.; Sun, F.; Jian, J.; Zhong, L.; Fang, Z.; Feng, J.; Yu, D., Alkene−Linked Covalent Organic Frameworks Boosting Photocatalytic Hydrogen Evolution by Efficient Charge Separation and Transfer in the Presence of Sacrificial Electron Donors. *Adv. Sci.* **2020,** *7* (12), 1902988.

19. Wang, K.; Yang, L.-M.; Wang, X.; Guo, L.; Cheng, G.; Zhang, C.; Jin, S.; Tan, B.; Cooper, A., Covalent Triazine Frameworks via a Low-Temperature Polycondensation Approach. *Angew. Chem. Int. Ed.* **2017,** *56* (45), 14149-14153.

20. Fang, X.; Shang, Q.; Wang, Y.; Jiao, L.; Yao, T.; Li, Y.; Zhang, Q.; Luo, Y.; Jiang, H.-L., Single Pt Atoms Confined into a Metal-Organic Framework for Efficient Photocatalysis. *Adv. Mater.* **2018,** *30* (7), 1705112.

21. He, T.; Chen, S.; Ni, B.; Gong, Y.; Wu, Z.; Song, L.; Gu, L.; Hu, W.; Wang, X., Zirconium–Porphyrin-Based Metal–Organic Framework Hollow Nanotubesfor Immobilization of Noble-Metal Single Atoms *Angew. Chem. Int. Ed.* **2018,** *57* (13), 3493–3498.

22. Liu, W.; Cao, L.; Cheng, W.; Cao, Y.; Liu, X.; Zhang, W.; Mou, X.; Jin, L.; Zheng, X.; Che, W.; Liu, Q.; Yao, T.; Wei, S., Single-Site Active Cobalt-Based Photocatalyst with a Long Carrier Lifetime for Spontaneous Overall Water Splitting. *Angew. Chem. Int. Ed.* **2017,** *56* (32), 9312-9317.